crystals

MDPI

Article

Wear and Corrosion Behaviour of Supersaturated Surface Layers in the High-Entropy Alloy Systems CrMnFeCoNi and CrFeCoNi

Thomas Lindner *, Martin Löbel, Erik Saborowski, Lisa-Marie Rymer and Thomas Lampke

Materials and Surface Engineering Group, Institute of Materials Science and Engineering, Chemnitz University of Technology, D-09107 Chemnitz, Germany; martin.loebel@mb.tu-chemnitz.de (M.L.); erik.saborowski@mb.tu-chemnitz.de (E.S.); lisa-marie.rymer@mb.tu-chemnitz.de (L.-M.R.); thomas.lampke@mb.tu-chemnitz.de (T.L.)

* Correspondence: th.lindner@mb.tu-chemnitz.de; Tel.: +49-371-531-38287

Received: 22 January 2020; Accepted: 10 February; Published: 12 February 2020

Abstract: The surface hardening of single-face-centred cubic (fcc)-phase CrMnFeCoNi and the manganese-free CrFeCoNi alloy was conducted using low-temperature nitrocarburisation. The microstructural investigations reveal the successful formation of a homogeneous diffusion layer with a thickness of approximately 16 µm. The interstitial solution of carbon and nitrogen causes an anisotropic lattice expansion. The increase in microhardness is in accordance to the graded concentration profile of the interstitial elements. Wear tests show a significantly enhanced resistance at different loads. The electrochemical tests reveal no deterioration in the corrosion resistance. The absence of precipitates is proven by microstructural investigations. The results prove the applicability of the concept of solution hardening by the formation of supersaturated solutions for the material group of high-entropy alloys. Hence, an increase of entropy with the consideration of lattice interstices provides new development approaches.

Keywords: high-entropy alloy; thermochemical treatment; surface hardening; supersaturated solution; wear; corrosion

1. Introduction

In recent years, the multi-component alloy concept of high-entropy alloys (HEAs) has received considerable attention [1]. Despite the absence of a main alloy constituent, promising material properties, e.g., high specific strength, high wear resistance and high oxidation and corrosion resistance have been proven [2–4]. The demands of superimposed loading require a complex profile of functional surface properties, resulting in a challenge for recent research activities in surface technology [5,6]. In general, single-phase HEAs like the CrMnFeCoNi HEA system with a face-centred-cubic (fcc) structure reveal good ductility and corrosion resistance, while a sufficient wear resistance is often associated to other compositions with body-centred-cubic (bcc)- or multi-phase constitution [7,8]. However, heterogeneous structures with a large variance of the local chemical composition often do not exhibit an adequate passivity and corrosion resistance [9]. An improvement of the relatively poor wear resistance of single-phase HEAs requires a functional division between surface and constructive properties. In this case, surface technologies are an appropriate opportunity to adjust the surface functionality.

Thermochemical treatments are suitable to enhance the performance of the surface layer region. The diffusion of elements causes the formation of solid solutions or precipitates. Thereby, the wear and corrosion resistance can be improved. Only few studies focusing on the surface hardening of HEAs have been conducted so far. Meng et al. have studied the nitriding of the duplex phase (fcc +

bcc) FeNiMnAlCr alloy system. The formation of a heterogeneous layer was proven [10]. Wang et al. investigated the plasma nitriding of the HEA system $Al_{1.3}CoCuFeNi_2$. However, metallographic investigations as well as phase analyses do not show clear evidence of a nitrided layer. Additionally, no significant improvement of the wear resistance was achieved [11,12]. Tang et al. conducted plasma nitriding of the bcc-phase HEA $Al_{0.5}CrFe_{1.5}MnNi_{0.5}$. Metallographic investigations prove the successful diffusion treatment by the formation of a nitride layer with a thickness of approximately 75 µm. Microhardness values of up to 1250 HV were achieved and the wear resistance was improved [13]. Lindner et al. performed a boriding treatment of CrMnFeCoNi as well as CrFeCoNi. Both alloys differ in the structural formation of the diffusion layer. A strong effect of the Ni content and of the donator composition is mentioned [14]. Accordingly, these studies prove a significant potential of hardening techniques for surface functionalisation. However, there is a considerable need for alloy specific process adjustments. Furthermore, the depletion of matrix elements can impair the corrosion resistance.

Solid solution strengthening using the interstices of the lattice can be an appropriate alternative to precipitation hardening. Moravcik et al. synthesised nitrogen alloyed CrMnFeCoNi HEAs by reactive powder milling. Precipitation occurs during spark plasma sintering of the powder, while the maximum solubility is stated as limiting factor [15]. Results of Xie et al. of doping CrMnFeCoNi powder with nitrogen reveal the formation of precipitates during vacuum hot pressing [16]. Alternatively, several research groups conducted the casting of HEAs. Wang et al. investigated the influence of the carbon content in the single-phase FeNiMnAlCr HEA system. Increasing the carbon concentration up to 1.1 at % results in a linear expansion of lattice parameter while precipitates are excluded [17]. Chen et al. doped $Fe_{40}Mn_{40}Co_{10}Cr_{10}$ with up to 8.9 at % carbon. A single-phase state and interstitial hardening were obtained up to a carbon concentration of 4.4 at %, whereas higher concentrations result in a decrease in lattice expansion by precipitate formation [18]. Shang et al. found that carbon additions in NiCoCr refine the dislocation substructure and increase the stacking fault energy, thereby decreasing the thickness of the twin bundles [19]. Moravcik et al. proved an increase in yield strength by interstitial nitrogen doping for the same alloy [20]. Zhang et al. found that adding yttrium can prevent boron precipitation promoting the solid solution strengthening effect induced by interstitial atoms. An fcc-phase microstructure provides a higher solubility. Moreover, laser cladding reliably inhibits boride precipitation in HEAs mainly composed of a bcc solid solution [21,22]. The different studies show a solid-solution strengthening effect. In particular, the fracture elongation is not affected unlike the common interstitial strengthening behaviour [17–22]. However, the effect on wear resistance is not investigated so far. Regarding the surface properties, thermochemical treatment can be an appropriate option for the enrichment of interstitial elements.

While precipitation hardening can affect the corrosion resistance, interstitial supersaturation of the matrix reliably prevents this. This behaviour has been proven in comprehensive investigations of stainless steels. The formation of HEAs with passive layers can be a promising opportunity for surface functionalisation. Therefore, the diffusion process has to be conducted below the critical temperature for precipitate formation respectively above their decomposition temperature [23].

Accordingly, the recent article investigates supersaturation hardening of single phase HEAs by thermochemical treatment. Phase formation and microstructural evolution in the surface layer region as well as the wear and corrosion behaviour are studied for the two single fcc-phase CrMnFeCoNi and CrFeCoNi HEA systems.

2. Materials and Methods

The two single-phase HEA-systems CrMnFeCoNi and CrFeCoNi were produced in equimolar composition using arc-melting of elemental granulates. The raw material provides a purity of over 99.9%. The arc melting process was carried out in a water-cooled copper crucible. Prior to the arc-melting process, the furnace chamber was evacuated and subsequently filled with argon. The arc was ignited using a tungsten electrode. To ensure chemical homogeneity, all samples were remolded three times including turning after each step. For a sample weight of 10 g, a cooling rate of < 50 K/s was determined for the furnace in preliminary studies. The manufacturing parameters are

summarised in Table 1. The chemical composition was analysed by X-ray fluorescence (XRF) FISCHERSCOPE X-RAY XAN (Helmut Fischer, Sindelfingen, Deutschland) with 30 kW and 1 mm collimator lens. The evaluation software Fischer XAN-WinFTM 6.33 was used. Each measurement was performed five times.

Table 1. Arc-furnace parameters.

Mean Quantity (g)	Droplet Size (mm)	Vacuum Pressure (mbar)	Argon Pressure (bar)	Gas Purity (%)	Current (A)
10	20	2×10^{-4}	1.1	99.9999	250

Slices with a thickness of 1.5 mm were cut out of the arc-melted samples using the Accutom 50 (Struers, Willich, Germany) device. The low temperature gasnitrocarburisation process was performed by BorTec GmbH and Co. KG (Hürth, Germany). Comparative investigations regarding the as-cast state were conducted. Metallographic cross-sections were prepared according to standard metallographic procedures. After hot mounting in conductive resin the grinded and polished cross-sections of the thermochemical treated samples were etched using Beraha-II colour etchant, to enable distinguishing of different microstructural domains in the surface layer region. An optical microscope GX51 (Olympus, Shinjuku, Japan) equipped with a SC50 camera (Olympus, Shinjuku, Japan) was used to study the distribution of the diffusion-enriched area. Furthermore, glow discharge optical emission spectroscopy (GDOS) was applied to determine the depth profile of the chemical composition. Therefore, a GDA750 analyzer (Spectruma Analytik GmbH, Hof, Germany) was used. The measurement was performed using a 2.5 mm anode, 800 V, 35 mA under 3 hPa argon pressure. Nanoindentation was performed for selective hardness measurements. A quasi-static measurement with a load of 1 mN was carried out using the nanoindenter UNAT (ASMEC GmbH, Radeberg, Germany) with a Berkovich tip. Vickers microhardness was deduced from the indentation depth using the InspectorX testing software version 3 (ASMEC GmbH, Radeberg, Germany). Crystallographic studies to identify the characteristic lattice parameters were conducted by X-ray diffraction (XRD) using a D8 DISCOVER diffractometer (Bruker AXS, Billerica, MA, USA) with Co-Kα radiation (tube voltage: 40 kV, tube current: 40 mA). The diffractometer was equipped with polycap optics for beam shaping, a 1 mm pinhole collimator and a 1D Lynxeye XE detector. The diffraction diagrams were measured in the diffraction angle (2θ) range from 20 to 130° with a step size of 0.01° and 3 s/step, which corresponds to 576 s/step due to the use of the 1D detector. The powder diffraction file (PDF) database 2014 was applied for phase identification. To investigate the wear behaviour ball-on-disk and reciprocating ball-on-plane tests were conducted. The applied parameters are summarised in Table 2.

Table 2. Parameters of the conducted wear tests.

Ball-on-Disk Test		Reciprocating Ball-on-Plane Test	
Force	20 N	Force	26 N
Radius	5 mm	Frequency	40 Hz
Speed	96 RPM	Time	900 s
Cycles	15916	Amplitude	0.5 mm
Counter body	Al_2O_3	Counter body	Al_2O_3
Diameter	6 mm	Diameter	10 mm

A Tetra Basalt Tester (Tetra, Ilmenau, Germany) and a Wazau SVT 40 device (Wazau, Berlin, Germany) were used for ball-on-disk and reciprocating ball-on-plane tests. The wear depth of the ball-on-disk tracks was determined by contact stylus instrument with a Hommel Etamic T8000 device (Jenotik, Villingen-Schwenningen, Germany). An optical 3D profilometer MikroCAD (LMI Technologies Inc., Burnaby, Canada) was used for the evaluation of the reciprocating ball-on-plane wear tracks. Current-density potential curves were recorded using 0.05 M H_2SO_4 and 0.5 M NaCl electrolyte for studying the passivation properties and pitting resistance, Table 3. With the used three-

electrode arrangement a round surface area with a diameter of 10 mm was tested. As a cathodic counter electrode, a platin sheet with the dimensions (2 × 2 cm²) was used. The reference was defined by the Ag/AgCl electrode with a potential of 207 mV compared to hydrogen, which was immersed into the Haber Lugging capillary with the different electrolytes. The tests were conducted at room temperature and the potential was recorded using a PS6 (Sensortechnik Meinsberg, Meinsberg, Deutschland) potentiometer.

Table 3. Parameters of the conducted corrosion tests.

	Passivation	**Pitting**
Electrolyte	0.05 M H_2SO_4	0.5 M NaCl
Potential-scan	-1000 to +1800 mV	-250 to +700 mV
	0.5 mV/s	0.1 mV/s

3. Results

3.1. Chemical Composition

The elemental compositions of the cast alloys are analysed by XRF measurement. The results are summarised in Table 4. In comparison to the intended equimolar composition, slight deviations can be determined. Especially, the chromium and manganese content are below the nominal values, which can be caused by evaporation of these elements in the arc-melting process. However, the obtained compositions were sufficiently accurate for further processing. Comparative measurements on the thermochemical treated samples revealed no deviation in elemental concentration. Hence, the absence of elemental segregation can be excluded, while nitrogen and carbon were below the detection limit of the XRF device.

Table 4. Average chemical composition of CrMnFeCoNi and CrFeCoNi in as-cast condition measured by X-ray fluorescence (XRF; main alloy elements in relative wt %).

	Co	**Cr**	**Fe**	**Mn**	**Ni**
CrMnFeCoNi	21.1	18.9	20.8	18.5	20.7
CrFeCoNi	26.0	23.0	25.6	-	25.4

GDOS measurements enable the investigation of the nitrogen and carbon distribution in the surface-layer region. The intensity levels of both elements were determined in dependence of sputter time. To obtain the surface distance of the elemental information, a series of spots were produced in increments of 100 seconds. 3D profilometry proves a homogeneous sputtering rate for both samples. Due to a lack of reference alloys, a reliable quantification of the element concentration is not possible. The intensity levels of nitrogen and carbon are plotted over the surface distance for the different alloys, Figure 1. A high nitrogen intensity was measured for the surface near area. While the nitrogen concentration decreases sharply with increasing distance to the surface, a plateau with a relatively constant intensity up to 22 µm and 15 µm occurs for the carbon intensity. The results prove a successful diffusion enrichment of the surface layer region. Manganese alloying does not affect the diffusion depth of nitrogen, while the carbon intensity indicates a higher diffusion depth for CoCrFeMnNi.

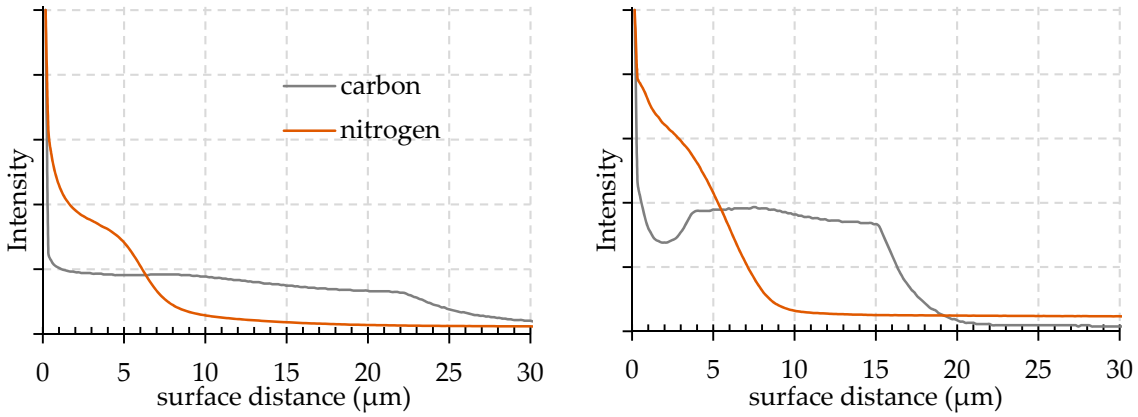

(a) CrMnFeCoNi **(b)** CrFeCoNi

Figure 1. Depth profile measured by glow discharge optical emission spectroscopy (GDOS) measurement.

3.2. Microstructural Analyses

The diffusion enrichment causes changes in the microstructure and property profile as well. In addition to the results of GDOS measurements, light microscopy of the cross-section enables the visualisation of local deviations in expression of diffusion depth. Colour contrasting using Beraha-II etchant enables a distinction between the diffusion layer and the unaffected material. Figure 2 illustrates the formation of the surface layer regarding the element composition. For both alloys, the formation of a dense surface layer free of cracks was proven. A homogeneous thickness was found for CrFeCoNi with a mean value of 16 µm. As a result of the manufacturing process, small cavities were observed within the manganese-containing alloy. These caused a deviation of the diffusion depth. Open porosity enabled the penetration of the donator during the diffusion enrichment process. Excluding this effect, a similar thickness was proven for both alloys. The results were in accordance with GDOS investigations, revealing a different behaviour for the alloys. The treatment temperatures of the thermochemical process strongly affected the diffusion speed. As a result, nitride layers in comparative work reach up to 75 µm in thickness [13]. Boride layers of the same alloy system show a thickness of 35 µm [14].

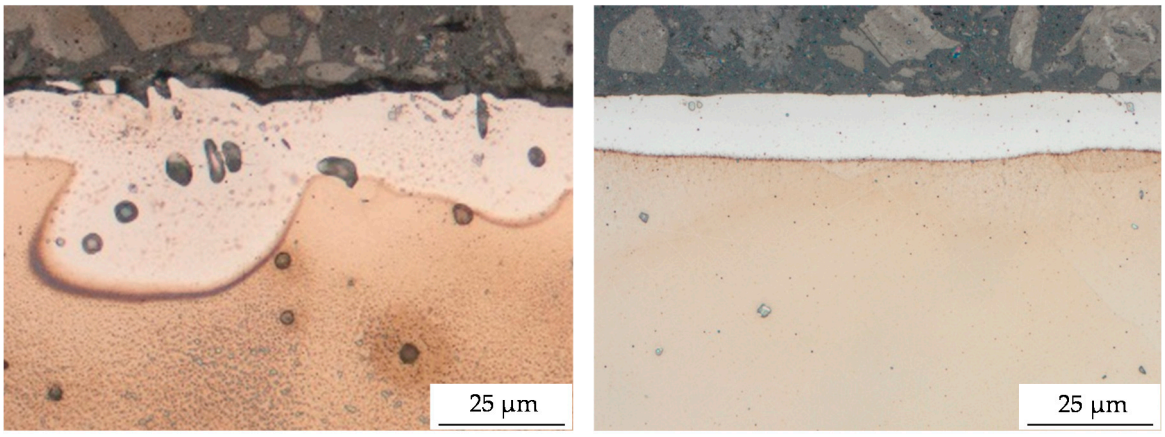

(a) CrMnFeCoNi **(b)** CrFeCoNi

Figure 2. Light microscopy images of nitrocarburised CrMnFeCoNi and CrFeCoNi high-entropy alloys (HEAs) in cross-section view of the surface layer using Beraha-II colour etchant.

XRD measurements have been conducted for the determination of the crystal structure and the lattice parameter. Figure 3 shows sections of the diffraction diagrams for the {111} and {200} lattice planes. The present phases have been assigned to the peaks for both alloys in as-cast and nitrocarburised state. The diffractograms of both alloys in as-cast state reveal another peak at 45.9°

due to the presence of the low-intensity Co Kβ radiation. Both alloys show a single-phase fcc-structure in the as-cast condition with a slight deviation in lattice parameter. For the manganese containing alloy CrMnFeCoNi a lattice parameter of a = 3.60 Å was calculated. The four-component system CrFeCoNi shows a minor decrease with a = 3.58 Å. In both cases, the low temperature nitrocarburisation process caused a change in microstructure. The absence of the peaks ascribed to the initial fcc-phase indicates a full transformation during the diffusion process. Two broad peaks appeared, which were shifted to lower diffraction angles in comparison to the former fcc-phase. This behaviour indicates a lattice expansion due to the interstitial solution of nitrogen and carbon. The formation of two peaks can be explained by a stronger expansion during interstitial solution of nitrogen compared to carbon. Hence, the expanded fcc-phases γ_N and γ_C with different lattice parameters appeared for both alloys. Table 5 summarises the shift of the lattice parameter for the gasnitrocarburised state in relation to the values of the as-cast state.

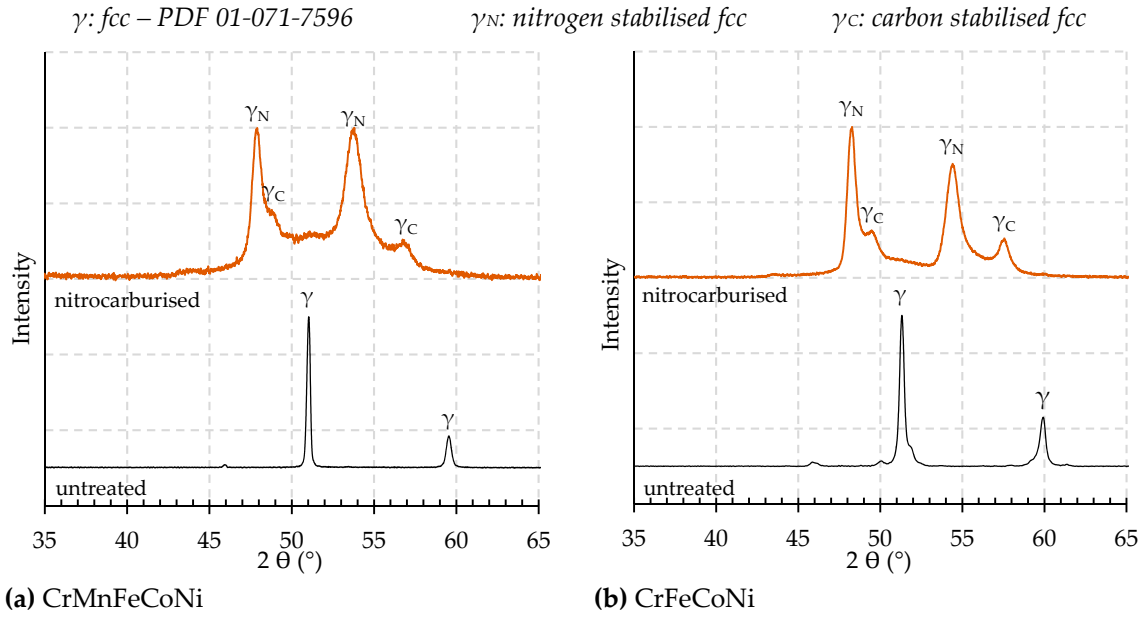

Figure 3. X-ray diffraction (XRD) diffractograms of the as-cast and nitrocarburised CrMnFeCoNi and CrFeCoNi HEAs.

A strong increase in lattice parameter was found. However, the expansion depends on the referenced lattice plane. According to the calculated values, a maximum relative lattice expansion of almost 10% was reached. The {200} planes show a significantly higher expansion compared to the {111} planes. A different expansion of the lattice planes {111} and {200} was expected as a consequence of the residual stress due to the anisotropic behaviour of Young's modulus. This is in accordance to the behaviour observed for stainless steel [24]. A slightly stronger increase was found for CrMnFeCoNi, which might be caused by a higher layer thickness.

Table 5. Lattice expansion determined for CrMnFeCoNi and CrFeCoNi depending on the lattice plane and the solved interstitial element (in Å).

	Lattice Plane	γ_N	γ_C
CrMnFeCoNi	{111}	0.24	0.14
	{200}	0.35	0.16
CrFeCoNi	{111}	0.22	0.11
	{200}	0.33	0.13

3.3. Microhardness and Wear Behaviour

Thermochemical treatment results in a strong increase in microhardness. Nanoindentation was performed on the surfaces and the cross-sections of the samples. The microhardness values of the cross-sections were determined above a surface distance of 7 µm to exclude edge influences. A higher microhardness of the base material was found for the manganese-alloyed system, while the manganese-free alloy shows a slightly higher hardness within the supersaturated surface layer, Figure 4. A gradual decrease in microhardness with increasing distance from the surface was found, whereas the maximum was about 1300 HV0.001. Corresponding to the micrographs in Figure 2 the microhardness decreased to the value of the base material at a surface distance of around 18 µm.

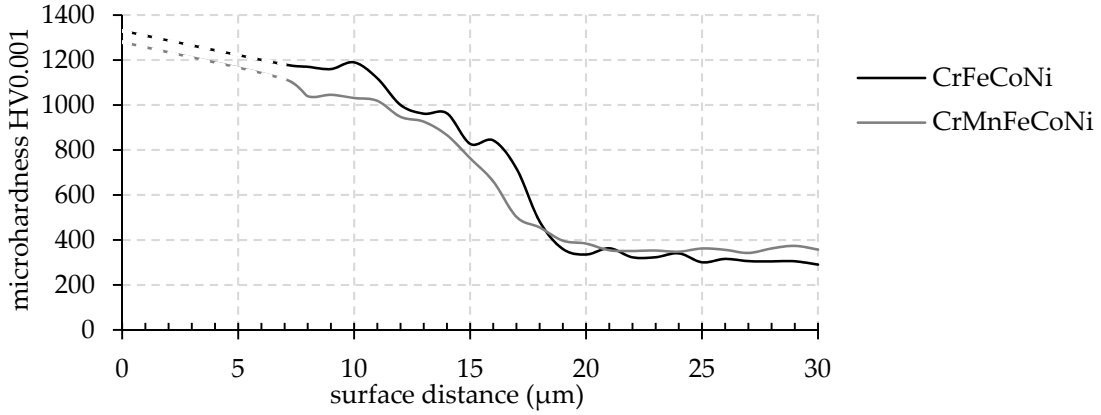

Figure 4. Microhardness of CrFeCoNi and CrMnFeCoNi in nitrocarburised state in dependence of the surface distance.

The results of comparative wear tests are shown in Figure 5. A strong increase in wear resistance for both alloys in nitrocarburised state was revealed. Under sliding wear conditions, the diffusion surface layer ensures a reliable wear protection. Furthermore, the wear depth and volume were significantly decreased under reciprocating ball-on-plane test conditions. Both alloys show a similar behaviour in ball-on-disk test, whereas a slightly higher wear could be observed for the manganese-free alloy under reciprocating test conditions.

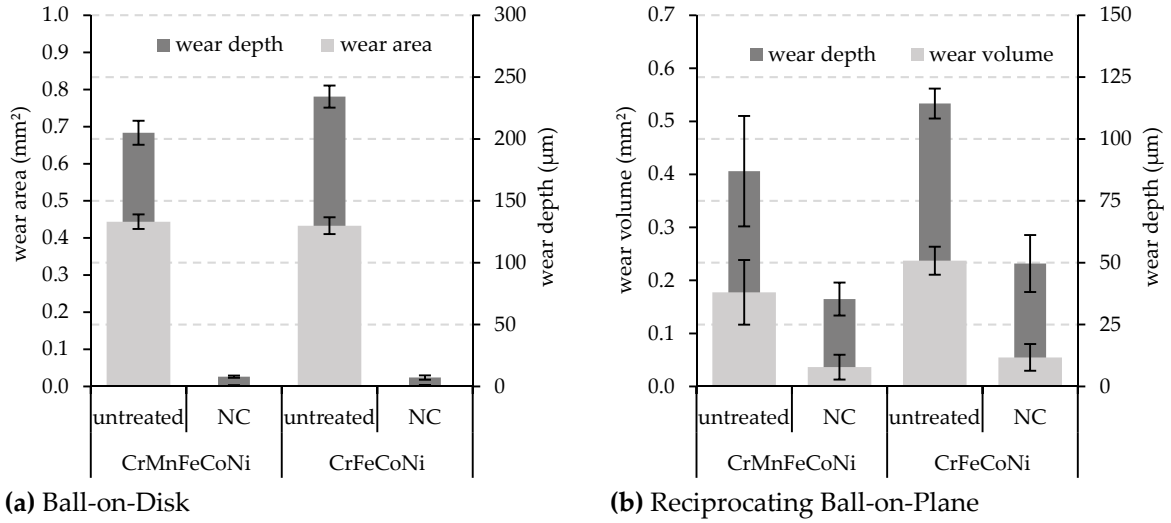

(a) Ball-on-Disk **(b)** Reciprocating Ball-on-Plane

Figure 5. Wear values of CrMnFeCoNi and CrFeCoNi in dependence of the treatment state and wear condition.

The wear tracks show only minor deviations, confirming a homogeneous state of the material properties. The alumina counter body exhibited no wear at all. With an average wear depth of 7 µm,

both alloys show an almost intact diffusion layer after ball-on-disk test. With a wear depth of 38 µm and 50 µm, the alternating wear exposure caused a degradation of the diffusion layer, resulting in less improvement. Therefore, a strong influence of the applied wear conditions could be concluded. In comparison to borided layers, the interstitial hardening provides advantages in case of the reciprocating test conditions [14]. The formation of the expanded austenitic phase by the interstitial solution of nitrogen and carbon results in a strong increase in microhardness and reliable improvement of wear resistance of the studied HEAs.

3.4. Corrosion Behaviour

Surface treatments can affect the corrosion resistance of materials. Especially precipitate formation can reduce the element concentration of chromium within the solid solution as a result of its high affinity to carbon and nitrogen [25]. Therefore, current-density potential curves where determined for different electrolyte types, Figure 6. The passivation properties were studied using H_2SO_4 electrolyte. An increase in the resting potential was observed for the thermochemically treated CrFeCoNi alloy. Both nitrocarburised samples show passivation, although their current density was approximately 100 times higher in comparison to the untreated state. Above 900 mV the untreated samples show a stronger increase. Hence, the current densities approach each other at about 1000 mV. However, a slight worsening in corrosion resistance could be concluded by the higher activity within the passivation range. The pitting corrosion tests with NaCl electrolyte revealed the opposite behaviour. While the resting potential was in the range of -30 to -140 mV, a lower gradient in current density increase was found for the nitrocarburised samples. The thermochemical treated CrFeCoNi sample even shows moderate current density at high potential. Therefore, an improvement of the resistance against pitting corrosion could be expected.

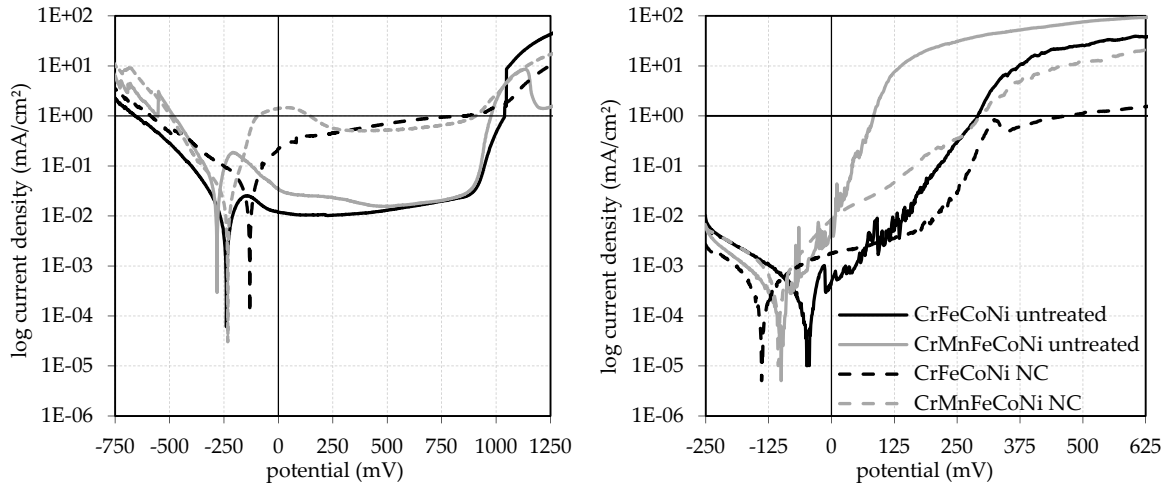

(a) 0.05 M H_2SO_4 electrolyte **(b)** 0.5 M NaCl electrolyte

Figure 6. Current-density potential curves of CrFeCoNi and CrMnFeCoNi in as-cast and nitrocarburised state tested with different electrolytes.

4. Summary

The first feasibility study proved the successful surface hardening of the fcc-phase HEAs by interstitial supersaturation of the solid solution using low temperature nitrocarburisation. The evolution of crystal structure and layer thickness were investigated in detail by microstructural and phase analyses. The elemental distribution within the surface layer was determined. Detailed information about mechanical, wear and corrosion properties were presented and discussed. The significant increase of wear resistance in combination with mainly unaffected corrosion properties for both HEAs underlines the suitability and application potential of the surface treatment. Manganese alloying of CrFeCoNi only results in a minor influence of the phase formation, while the formation of structural defects, e.g., pores, directly influences the diffusion depth. Excluding the

effect of structural influences, a diffusion depth of about 16–18 μm was confirmed for both alloys by nanoindentation and colour etching of the surface layer. The current study presents a suitable route to circumvent the drawbacks of low hardness and wear resistance inherent to fcc high-entropy alloys.

Author Contributions: T.L., M.L. and L.-M.R. conceived and designed the experiments. T.L., M.L. and E.S. performed the experiments, analysed the data and wrote the paper. T.L. directed the research and contributed to the discussion and interpretation of the results. All authors have read and agreed to the published version of the manuscript.

Funding: This study was funded via Sächsische Aufbaubank - Förderbank/SAB-100382175 by the European Social Fund ESF and the Free State of Saxony as well as by the German Research Foundation (Deutsche Forschungsgemeinschaft/DFG) project number La-1274/54-1. The publication of this article was funded by Chemnitz University of Technology.

Acknowledgments: The authors thank Ralph Hunger from company of BorTec for performing the thermochemical treatment. The support by Thomas Mehner, Paul Clauß, Steffen Clauß and Elke Benedix (all from the Institute of Materials Science and Engineering) is gratefully acknowledged.

Conflicts of Interest: The authors declare no conflict of interest.

References

1. Miracle, D.B. High-Entropy Alloys: A Current Evaluation of Founding Ideas and Core Effects and Exploring ''Nonlinear Alloys''. *JOM* **2017**, *69*, 2130–2136, doi:10.1007/s11837-017-2527-z.
2. Yao, H.; Tan, Z.; He, D.; Zhou, Z.; Zhou, Z.; Xue, Y.; Cui, L.; Chen, L.; Wang, G.; Yang, Y. High strength and ductility AlCrFeNiV high entropy alloy with hierarchically heterogeneous microstructure prepared by selective laser melting. *J. Alloy. Compd.* **2020**, *813*, 152196, doi:10.1016/j.jallcom.2019.152196.
3. Moravcik, I.; Cizek, J.; Kovacova, Z.; Nejezchlebova, J.; Kitzmantel, M.; Neubauer, E.; Kubena, I.; Hornik, V.; Dlouhy, I. Mechanical and microstructural characterization of powder metallurgy CoCrNi medium entropy alloy. *Mater. Sci. Eng. A* **2017**, *701*, 370–380, doi:10.1016/j.msea.2017.06.086.
4. Fazakas, E.; Varga, B.; Geantă, V.; Berecz, T.; Jenei, P.; Voiculescu, I.; Coșniță, M.; Ștefănoiu, R. Microstructure, Thermal, and Corrosion Behavior of the AlAgCuNiSnTi Equiatomic Multicomponent Alloy. *Materials* **2019**, *12*, 926, doi:10.3390/ma12060926.
5. Chen, L.; Bobzin, K.; Zhou, Z.; Zhaob, L.; Öte, M.; Königstein, T.; Tan, Z.; He, D. Wear behavior of HVOF-sprayed $Al_{0.6}$TiCrFeCoNi high entropy alloy coatings at different temperatures. *Surf. Coat. Technol.* **2019**, *358*, 215–222, doi:10.1016/j.surfcoat.2018.11.052.
6. Löbel, M.; Lindner, T.; Mehner, T.; Lampke, T. Microstructure and Wear Resistance of AlCoCrFeNiTi High-Entropy Alloy Coatings Produced by HVOF. *Coatings* **2017**, *7*, 144, doi:10.3390/coatings7090144.
7. Löbel, M.; Lindner, T.; Mehner, T.; Dietrich, D.; Lampke, T. Influence of Titanium on Microstructure, Phase Formation and Wear Behaviour of $AlCoCrFeNiTi_x$ High-Entropy Alloy. *Entropy* **2018**, *20*, 505, doi:10.3390/e20070505.
8. Kong, D.; Guo, J.; Liu, R.; Zhang, X.; Song, Y.; Li, Z.; Guo, F.; Xing, X.; Xu, Y.; Wang, W. Effect of remelting and annealing on the wear resistance of $AlCoCrFeNiTi_{0.5}$ high entropy alloys. *Intermetallics* **2019**, *114*, 106560.
9. Wang, W.; Wang, J.; Sun, Z.; Li, J.; Li, L.; Song, X.; Wen, X.; Xie, L.; Yang, X. Effect of Mo and aging temperature on corrosion behavior of $(CoCrFeNi)_{100-x}Mo_x$ high-entropy alloys. *J. Alloy. Compd.* **2020**, *812*, 152139, doi:10.1016/j.jallcom.2019.152139.
10. Meng, F.; Baker, I. Nitriding of a high entropy FeNiMnAlCr alloy. *J. Alloy. Compd.* **2015**, *645*, 376–381, doi:10.1016/j.jallcom.2015.05.021.
11. Wang, Y.; Yang, Y.; Yang, H.; Zhang, M.; Qiao, J. Effect of nitriding on the tribological properties of $Al_{1.3}CoCuFeNi_2$ high-entropy alloy. *J. Alloy. Compd.* **2017**, *725*, 365–372, doi:10.1016/j.jallcom.2017.07.132.
12. Wang, Y.; Yang, Y.; Yang, H.; Zhang, M.; Ma, S.; Qiao, J. Microstructure and wear properties of nitrided AlCoCrFeNi high-entropy alloy. *Mater. Chem. Phys.* **2018**, *210*, 233–239, doi:10.1016/j.matchemphys.2017.05.029.
13. Tang, W.-Y.; Chuang, M.-H.; Chen, H.-Y.; Yeh, J.-W. Microstructure and mechanical performance of new $Al_{0.5}CrFe_{1.5}MnNi_{0.5}$ high-entropy alloys improved by plasma nitriding. *Surf. Coat. Technol.* **2010**, *204*, 3118–3124, doi:10.1016/j.surfcoat.2010.02.045.

14. Lindner, T.; Löbel, M.; Sattler, B.; Lampke, T. Surface hardening of FCC phase high-entropy alloy system by powder-pack boriding. *Surf. Coat. Technol.* **2019**, *371*, 389–394.
15. Moravcik, I.; Cizek, J.; Gouvea, L.D.A.; Cupera, J.; Guban, I.; Dlouhy, I. Nitrogen Interstitial Alloying of CoCrFeMnNi High Entropy Alloy through Reactive Powder Milling. *Entropy* **2019**, *21*, 363, doi:10.3390/e21040363.
16. Xie, Y.; Cheng, H.; Tang, Q.; Chen, W.; Dai, P. Effects of N addition on microstructure and mechanical properties of CoCrFeNiMn high entropy alloy produced by mechanical alloying and vacuum hot pressing sintering. *Intermetallics* **2018**, *93*, 228–234, doi:10.1016/j.intermet.2017.09.013.
17. Wang, Z.; Baker, I.; Cai, Z.; Chen, S.; Poplawsky, J.D.; Guo, W. The effect of interstitial carbon on the mechanical properties and dislocation substructure evolution in $Fe_{40.4}Ni_{11.3}Mn_{34.8}Al_{7.5}Cr_6$ high entropy alloys. *Acta Mater.* **2016**, *120*, 228–239, doi:10.1016/j.actamat.2016.08.072.
18. Chen, L.B.; Wei, R.; Tang, K.; Zhang, J.; Jiang, F.; He, L.; Sun, J. Heavy carbon alloyed FCC-structured high entropy alloy with excellent combination of strength and ductility. *Mater. Sci. Eng.* **2018**, *716*, 150–156, doi:10.1016/j.msea.2018.01.045.
19. Shang, Y.Y.; Wu, Y.; He, J.Y.; Zhu, X.Y.; Liu, S.F.; Huang, H.L.; An, K.; Chen, Y.; Jiang, S.H.; Wang, H.; et al. Solving the strength-ductility tradeoff in the medium-entropy NiCoCr alloy via interstitial strengthening of carbon. *Intermetallics* **2019**, *106*, 77–87, doi:10.1016/j.intermet.2018.12.009.
20. Moravcik, I.; Hadraba, H.; Li, L.; Dlouhy, I.; Raabe, D.; Li, Z. Yield strength increase of a CoCrNi medium entropy alloy by interstitial nitrogen doping at maintained ductility. *Scr. Mater.* **2020**, *178*, 391–397, doi:10.1016/j.scriptamat.2019.12.007.
21. Zhang, H.; Zhong, X.C.; He, Y.Z.; Li, W.H.; Wu, W.F.; Chen, G.; Guo, S. Effect of High Configuration Entropy and Rare Earth Addition on Boride Precipitation and Mechanical Properties of Multi-principal-Element Alloys. *J. Mater. Eng. Perform.* **2017**, *26*, 3750–3755, doi:10.1007/s11665-017-2831-3.
22. Zhang, H.; Tang, H.; He, Y.Z.; Zhang, J.L.; Li, W.H.; Guo, S. Effect of Heat Treatment on Borides Precipitation and Mechanical Properties of CoCrFeNiAl1.8Cu0.7B0.3Si0.1 High-Entropy Alloy Prepared by Arc-Melting and Laser-Cladding. *JOM* **2017**, *69*, 2078–2083, doi:10.1007/s11837-017-2381-z.
23. Valente, E.H.; Christiansen, T.; Somers, M. High-Temperature Solution Nitriding and Low-Temperature Surface Nitriding of 3D Printed Stainless Steel. In Proceedings of the Conference: ECHT—European Conference on Heat Treatment, 2018; pp. 71–80. Available online: https://www.researchgate.net/publication/324941781 (accessed on 1. January.2020).
24. Moskalioviene, T.; Galdikas, A. Kinetic model of anisotropic stress assisted diffusion of nitrogen in nitrided austenitic stainless steel. *Surf. Coat. Technol.* **2019**, *366*, 277–285, doi:10.1016/j.surfcoat.2019.03.054.
25. Zhang, Z.L.; Bell, T. Structure and Corrosion Resistance of Plasma Nitrided Stainless Steel. *Surf. Eng.* **1985**, *1*, 2, doi:10.1179/sur.1985.1.2.131.